A model to predict the elastic properties of gas hydrate-bearing sediments

Tuan Nguyen-Sy, Anh Minh A.M. Tang, Quy-Dong To, Minh Ngoc Vu

A model to predict the elastic properties of gas hydrate-bearing sediments

Tuan Nguyen-Sy[a,b], Anh-Minh Tang[c], Quy-Dong To[d], Minh-Ngoc Vu[d]

(a) *Division of Construction Computation, Institute for Computational Science, Ton Duc Thang University, Ho Chi Minh City, Vietnam.*
(b) *Faculty of Civil Engineering, Ton Duc Thang University, Ho Chi Minh City, Vietnam*

(c) Ecole des Ponts ParisTech, Marne-la-Vallée, France

(d) Duy Tan University, Institute of Research and Development, 03 Quang Trung, Danang, Vietnam

Corresponding author: nguyensytuan@tdtu.edu.vn

Abstract: A simple and accurate model for predicting the elastic properties of gas hydrate-bearing sediment (GHBS) is proposed and validated against experimental data. It is developed on the basis of the homogenization theory for multiphase composite. Unlike the classical homogenization techniques those fix a homogenization scheme (*e.g.* self-consistent, Mori-Tanaka, DEM, *etc*.) for a given microstructure, the proposed model considers a flexible homogenization scheme that adapts with the change of the microstructure of the material. The idea is to modify the elastic properties of the reference matrix with respect to the microstructure change of the mixture. Such modification is ensured by adapting the theoretical method to available experimental data. The derived method is proved to be very powerful as it can fit laboratory measured data on gas hydrate-bearing sand formed by different methods including excess gas and excess water methods and log data taken from various sites. Such feature cannot be satisfied by the existent models those consider the hydrate phase as a cement phase or a pore-filling phase. A very good agreement between the proposed method and experimental data offer a simple and accurate ways to predict the saturation of gas hydrate using sonic log data or 3D seismic data.

Keywords: gas hydrate-bearing sediment; elastic properties; homogenization; adaptive scheme

1. Introduction

Gas hydrate-bearing sediment (GHBS) is an energy resource made of low molecular weight gas (methane) hosted by hydrogen-bonded water filling in the porous space between the solid

sediment grains (Milkov, 2004; Sloan and Koh, 2007; Waite et al., 2009; Rees et al., 2011). The dissociation of gas hydrate in sediment nearby a borehole yields the change of the in situ pore pressure and stress as well as the modification of the mechanical properties of the GHBS (Li et al., 2011; Le et al., 2019). These phenomena can lead to serious stability problems (Tan et al., 2005; Rutqvist and Moridis, 2007; Freij-Ayoub et al., 2007).

The gas hydrate content acts as a lightweight solid content that decreases the hydraulic conductivity and increases the elastic stiffness and the sonic wave velocities of the GHBS comparing to equivalent sediment without gas hydrate (Priest et al., 2005; Johnson et al., 2011). Therefore sonic log data can be used to estimate hydrate saturation (Guerin et al., 1999).

A number of models were proposed to predict the elastic and sonic properties of GHBS. Lee et al. (1996) proposed a simple weighted equation to estimate the hydrate saturation using compressional and shear sonic wave velocities (see also Lee and Collett, 2001; Lee, 2002). Carcione and Tinivella (2000) use a Biot-type three-phase model including two solid phases to model the sonic velocities of GHBS. Helgerud et al. (1999) considered an effective medium theory that was previously developed by Dvorkin and Nur (1996) for sandstone to model GHBS. This later considered the contact Hertz-Mindlin model for a granular packing at a critical porosity of about 0.36 to 0.40 and then the Hashin-Shtrikman formulas (Hashin and Shtrikman, 1963) to estimate the effective bulk and shear moduli at porosities higher or lower than the critical porosity. Then the Gassmann's theory (Gassmann, 1951) was employed to relate the dry and saturated moduli. In this model, the hydrate content was regarded by two possibilities: hydrate was associated to the solid phase or the fluid phase. This idea was also considered by Jakobsen et al. (2000) in an anisotropic Self-Consistent (SC) and Differential Effective Medium (DEM) approximation (combined SC-DEM method). For the assumption of hydrate associated to the solid phase, they started by considering the self-consistent scheme for the mixture of solid grains and hydrate, then the multi-step DEM procedure was used to replace a little amount of hydrate by water in each step. The role of hydrate and water were interchanged if hydrate was considered as part of the fluid phase. This model was considered by Chand et al. (2004, 2006) for the computation of the hydrate saturation in GHBS from sonic data. However, when comparing the results predicted by the SC-DEM method with experimental data, we observe that it strongly over-estimates the elastic properties and the sonic velocities of gas hydrate-bearing sediments. Indeed, such method can be used for highly compacted rocks such as shale or sandstone those are buried deeply in the sediments but it is not appropriate for gas hydrate-bearing sediments those are usually located at a shallow buried depth.

Recently, a new and powerful homogenization concept was proposed to deal with the effective physical properties of composite containing highly contrast phases (Nguyen et al., 2016). It was a flexible homogenization technique that could smoothly transfer from one homogenization scheme to another by modifying the properties of the reference matrix with respect to the microstructure of the whole medium. It was demonstrated that experimental data can be perfectly fitted by such method.

In the present work, the concept proposed by Nguyen et al. (2016) is applied to predict the elastic and sonic properties of GHBS. After a review of experimental observations, the theoretical basis of the homogenization is briefly presented. Afterward, the homogenization scheme is calibrated and validated against experimental data collected from literature. The sensitivity of the model's parameters is analyzed. The robustness of the model to predict the sonic properties of GHBS is finally discussed.

2. Review of experimental observations

Several experimental data on the elastic and sonic properties of GHBS can be found in literature. For example, Priest et al. (2005) measured the compressional and shear wave velocities of gas hydrate-bearing sand samples formed by the technique proposed by Stern et al. (1996). Their measurements were performed at low frequencies and small strain amplitude corresponding to the range of field seismic acquisition. They observed a strong increase of the sonic velocities versus increasing of hydrate saturation. The stress dependence of the sonic velocities, observed for sand packing and sandstone without gas hydrate, was also observed for gas hydrate-bearing sand. Such observation suggests that the role of grain-to-grain contact is also important for GHBS. Yun et al. (2005) measured the compression and shear sonic wave velocities of tetrahydrofuran (THF) gas hydrate-bearing sand. This latter was formed from water saturated sand packing by decreasing the temperature at low confining pressure condition (see also Choi et al, 2014; Sultaniya et al., 2015). They observed that the dependence of the sonic wave velocities on the hydrate saturation of GHBS was a lot less significant than that formed by Priest et al. (2005). It was confirmed by Priest et al. (2009) that the elastic wave velocities of GHBS were strongly affected by its morphology. Indeed, the hydrate-bearing sand formed by "excess gas" method (Priest et al., 2005) created cement gas-hydrate morphology while the "excess water" method considered by Yun et al. (2005) and Priest et al. (2009) created pore-filling gas-hydrate morphology. Hu et al. (2012) created methane hydrate-bearing sand sediment by injecting directly high-pressure methane gas into natural sand saturated with a 300 ppm Sodium dodecyl sulfate (SDS) solution. Konno et al. (2015) measured the compressional

wave velocity of natural sandy sediments at near in-situ pressures and temperatures and found that the wave velocity correlated well with the hydrate saturation. To summary, there are three main methods to create gas hydrate in laboratory: (i) excess water hydrate formation; (ii) excess gas hydrate formation; and (iii) hydrate formation out of solution. At low saturations, excess gas produces strongly cementing hydrates while excess water and solution techniques produce pore filling hydrates. As the hydrate saturations increase, the hydrate becomes continuously more cementing (see Rydzy, 2015).

So it is clear that the sonic velocities of GHBS strongly depended on the ways it was formed (Yun et al., 2005; Priest et al., 2005, 2009; Rydzy, 2014) and were different from field data (Lee et al., 1996; Lee and Collett, 2001; Lee, 2008). *Figure 1* and *Figure 2* show the compressional and shear sonic wave velocities (*Vs* and *Vp*, respectively), of different gas hydrate-bearing sand formed in laboratory and natural GHBS, versus the hydrate saturation degree as well as a cross-plot between these velocities. Yun et al. (2005) used THF-hydrate instead of methane hydrates because it has similar thermo-mechanical properties to and the same molecular structure (Structure II) as hydrates of most thermogenic gases. In addition, from the micromechanical point of view, the elastic properties of THF and methane hydrates are similar when compared to that of quartz. Data obtained for sandstone and natural sand without gas hydrate (Han et al., 1986; Devorkin and Nur, 1996) are also plotted for comparison. At a low velocity range, corresponding to low hydrate saturation, the shear velocity at a given compressional velocity obtained in laboratory by excess gas method (Priest et al., 2005) is a lot higher than the shear velocity obtained by the excess water method (Yun et al., 2005; Priest et al., 2009). Note that Yun et al. (2005) saturated fine-grained sand specimen by water-THF solutions to form hydrate whereas Priest et al. (2009) injected de-aired water into air-dried fine-grained sand specimen saturated with methane gas. Actually, after Priest et al. (2009), the excess gas method forms gas hydrate at the grain contacts (cementing) while the excess water one allows gas hydrate to form within the pore space between the sand grains (pore-filling). In addition, within the excess water method, at higher hydrate saturation, the hydrate forms at the grain contact (cementing) although hydrate starts to form as pore-filling. For this reason, the results obtained by the excess water method approach those of excess gas method at higher saturation. Some laboratory gas-hydrate forming techniques provide data in between these two limits. For instance, Zhang et al. (2011) formed gas hydrate-bearing sand starting from partially water saturated sand packing and observed that the gas hydrate started to be a pore-filling phase at the beginning and then became the cement content at the end. Of cause other factors such as

the stress condition, mineralogy and fluid type must affect the effective elastic and sonic properties of GHBS. But for a given mineralogy and fluid type at a fixed stress state, it is obvious that the morphology of the gas-hydrate content must play a crucial role.

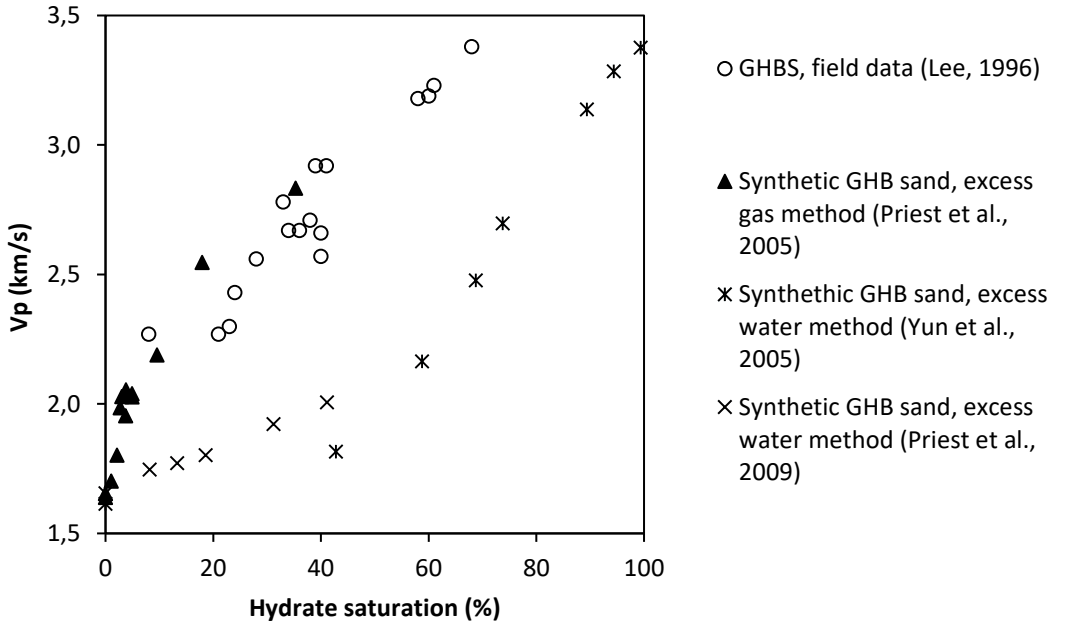

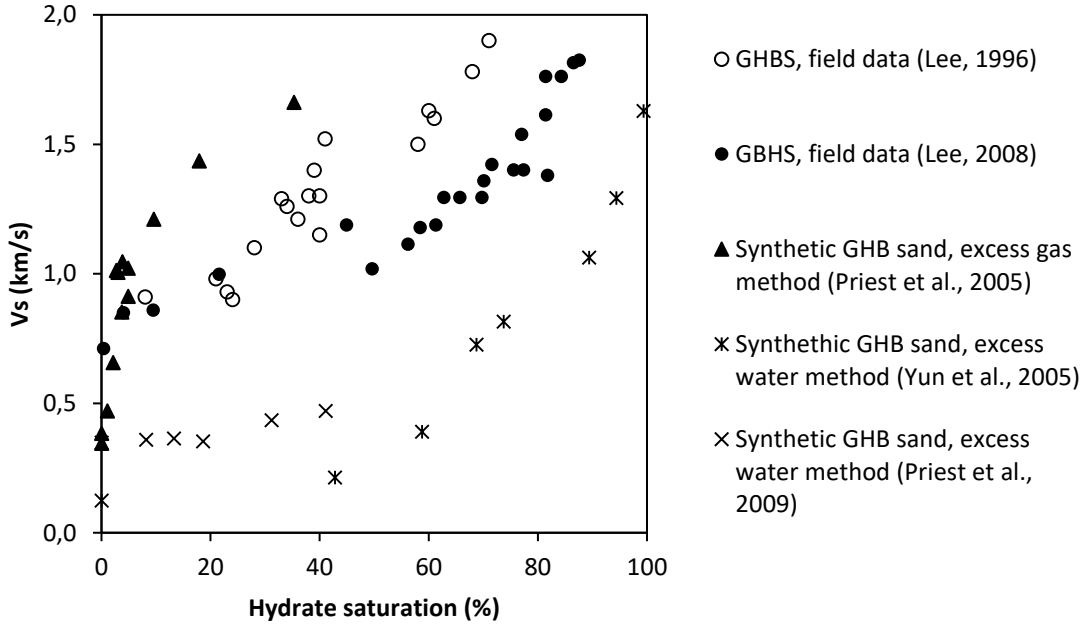

Figure 1: Compressional and shear sonic velocities of GHBS versus hydrate saturation: experimental and field data.

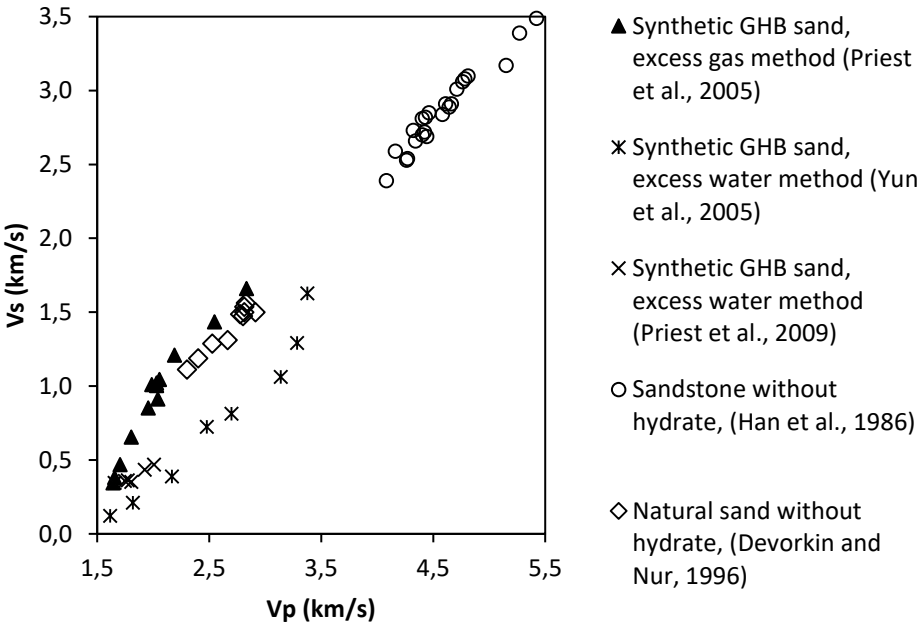

144

145 *Figure 2: Shear sonic velocity (Vs) versus compression sonic velocity (Vp) of gas hydrate-*
146 *bearing sands and those without gas hydrate.*

147

148 **3. Review of the theoretical basis**

149 The homogenization theory allows modeling effective elastic (and/or transport) properties
150 of a heterogeneous medium. It starts by considering an elementary problem of a single
151 heterogeneity in an infinite medium (dilute problem, Eshelby, 1957). Then Mori-Tanaka theory
152 (Mori and Tanaka, 1973) allows extending dilute solution to a medium containing many
153 inclusions those are interacted. However Mori-Tanaka scheme is limited to a matrix-inclusion
154 system with a low to medium volume fraction of inclusions. Therefore it is not appropriate for
155 a rock that is not a matrix-inclusion system. In such situation, it is required to define an
156 equivalent matrix of the medium. For example, the self-consistent scheme considers the
157 homogenized medium itself as the matrix of the mixture. But this method has also little
158 application for rocks because it usually over-estimates the elastic properties due to the strong
159 contrast between the solid and the fluid phases. A more sophisticated definition of the matrix is
160 required to appropriately modeling elastic (and transport) properties of rock (e.g. Nguyen et al.,
161 2016)

162 This section provides the basic elements of the homogenization theory for isotropic
163 composite with a highlight on the flexible homogenization concept previousely proposed by

Nguyen et al. (2016). The local relationship between the stress tensor $\boldsymbol{\sigma}$ and strain tensor $\boldsymbol{\varepsilon}$ is defined by the following linear elastic equation:

$$\boldsymbol{\sigma} = \mathbb{C}: \boldsymbol{\varepsilon} \tag{1}$$

where $\mathbb{C}$ is the fourth order local stiffness tensor; the column ":" is for a double contraction of two tensors. The macroscopic behavior of a representative elementary volume (REV) is:

$$\langle \boldsymbol{\sigma} \rangle = \mathbb{C}^{hom}: \langle \boldsymbol{\varepsilon} \rangle \tag{2}$$

where the notation $\langle . \rangle$ stands for a volumetric average over the REV; the superscript "hom" is for a homogenized term. The local and average strains are related via the strain localization tensor such as:

$$\boldsymbol{\varepsilon} = \mathbb{A}: \langle \boldsymbol{\varepsilon} \rangle \tag{3}$$

where $\mathbb{A}$ is the strain localization (or concentration) tensor that is a function of the mechanical properties, the volume fraction and the shape of the phases as well as the interaction between them. By combining equations **(1)** to **(3)**, the effective stiffness tensor $\mathbb{C}^{hom}$ can be related to the local stiffness tensors as:

$$\mathbb{C}^{hom} = \langle \mathbb{A}: \mathbb{C} \rangle \tag{4}$$

According to Mori and Tanaka (1973), the localization tensor $\mathbb{A}$ can be expressed as:

$$\mathbb{A} = \mathbb{A}^{dl} \langle \mathbb{A}^{dl} \rangle^{-1} \tag{5}$$

where $\mathbb{A}^{dl}$ is the dilute localization tensor of a matrix-inclusion system that has been well etablished by Eshelby (1957):

$$\mathbb{A}^{dl} = [\mathbb{I} + \mathbb{P}_0 (\mathbb{C}_{inc} - \mathbb{C}_0)]^{-1} \tag{6}$$

where $\mathbb{C}_{inc}$ is the elastic stiffness tensor of the inclusion; $\mathbb{C}_0$ the elastic stiffness tensor of the reference matrix; $\mathbb{P}_0$ the Hill's tensor that is a function of $\mathbb{C}_0$ and the shape of the inclusion; $\mathbb{I}$ the fourth order identity tensor. For the case of isotropic matrix and inclusion, the stiffness tensors $\mathbb{C}_{inc}$ and $\mathbb{C}_0$ can be expressed in term of the bulk and shear moduli such as:

$$\mathbb{C}_{inc} = 3k_{inc}\mathbb{J} + 2\mu_{inc}\mathbb{K};\ \mathbb{C}_0 = 3k_0\mathbb{J} + 2\mu_0\mathbb{K} \tag{7}$$

where $\mathbb{J}$ and $\mathbb{K}$ are the spherical and deviatoric part of the identity tensor $\mathbb{I}$: $\mathbb{I} = \mathbb{J} + \mathbb{K}$; k_{inc} and μ_{inc} the bulk and shear moduli of the inclusion; k_0 and μ_0 the bulk and shear moduli of the reference matrix.

The assumption of spherical inclusion is usually considered for sandstone. Such assumption yields following simple formula of the Hill's tensor (Dormieux et al., 2006):

$$\mathbb{P}_0 = \frac{1}{3(k_0 + a_0)}\mathbb{J} + \frac{1}{2(\mu_0 + b_0)}\mathbb{K} \tag{8}$$

where

$$a_0 = \frac{4}{3}\mu_0;\ b_0 = \frac{\mu_0(9k_0 + 8\mu_0)}{6(k_0 + 2\mu_0)} \tag{9}$$

Using the formula (**7)** for the elastic stiffness tensors of the matrix and inclusion and the formulas (**8)** and (**9)** for the Hill's tensor, equation (**6)** yields the following formula of an isotropic dilute localization tensor:

$$\mathbb{A}^{dl} = \frac{k_0 + a_0}{k_{inc} + a_0}\mathbb{J} + \frac{\mu_0 + b_0}{\mu_{inc} + b_0}\mathbb{K} \tag{10}$$

Then equation (**5)** yields:

$$\mathbb{A} = \frac{k_0 + a_0}{k_{inc} + a_0}\langle\frac{k_0 + a_0}{k + a_0}\rangle^{-1}\mathbb{J} + \frac{\mu_0 + b_0}{\mu_{inc} + b_0}\langle\frac{\mu_0 + b_0}{\mu + b_0}\rangle^{-1}\mathbb{K} \tag{11}$$

where k and μ, which appear inside the average operator $\langle . \rangle$, stand for the bulk and shear moduli of a component (matrix or inclusion). Note that the terms with index 0 can be put out of the volumetric average terms, therefore the localization tensor can be simplified to:

$$\mathbb{A} = \frac{1}{k_{inc} + a_0}\langle\frac{1}{k + a_0}\rangle^{-1}\mathbb{J} + \frac{1}{\mu_{inc} + b_0}\langle\frac{1}{\mu + b_0}\rangle^{-1}\mathbb{K} \tag{12}$$

Finally, the introduction of equation (**11)** in equation (**4)** provides the following formula of the elastic stiffness tensor:

$$\mathbb{C}^{hom} = \langle 3k\frac{1}{k + a_0}\rangle\langle\frac{1}{k + a_0}\rangle^{-1}\mathbb{J} + \langle 2\mu\frac{1}{\mu + b_0}\rangle\langle\frac{1}{\mu + b_0}\rangle^{-1}\mathbb{K} \tag{13}$$

That can be recast in the form:

$$\mathbb{C}^{hom} = 3k_{hom}\mathbb{J} + 2\mu_{hom}\mathbb{K} \tag{14}$$

where the homogenized bulk and shear moduli, k_{hom} and μ_{hom}, are (see also Pham et al., 2017):

$$k_{hom} = \langle \frac{k}{k + a_0} \rangle \langle \frac{1}{k + a_0} \rangle^{-1} = \langle \frac{1}{k + a_0} \rangle^{-1} - a_0 \quad (15)$$

and

$$\mu_{hom} = \langle \frac{\mu}{\mu + b_0} \rangle \langle \frac{1}{\mu + b_0} \rangle^{-1} = \langle \frac{1}{\mu + b_0} \rangle^{-1} - b_0 \quad (16)$$

The choice of the parameters a_0 and b_0 of the reference matrix depends on the homogenization scheme chosen. For example, the self-consistent scheme corresponds to computing a_0 and b_0 using equation (**9)** in which the effective bulk and shear moduli are used as the bulk and shear moduli of the reference matrix, i.e. $k_0 = k_{hom}$ and $\mu_0 = \mu_{hom}$. The Mori-Tanaka scheme is usually used for a composite containing a major connected phase that can be considered as the reference matrix of which the elastic bulk and shear moduli can be used to compute the parameters a_0 and b_0. In the multi-step differential effective medium (DEM) scheme, a_0 and b_0 of a step *n* are computed from the effective bulk and shear moduli obtained at the previous step $(n-1)$.

The main idea of the homogenization scheme proposed by Nguyen et al. (2016) is to let the parameters a_0 and b_0 change flexibly according to the change of the microstructure. Such correlation between the properties of the reference matrix and the microstructure can be calibrated by inverse analysis regarding available experimental data. Details of this model for the case of GHBS are presented in subsequent section.

4. Application for gas hydrate-bearing sand

4.1. The model

Considering water saturated gas hydrate-bearing sand that can be modeled by a mixture of three phases: quartz grains, gas hydrate and water. Applying the formulas (**15)** and (**16)**, we have:

$$k_{hom} = \left[\frac{f_q}{k_q + a_0} + \frac{f_h}{k_h + a_0} + \frac{f_w}{k_w + a_0} \right]^{-1} - a_0 \quad (17)$$

and

$$\mu_{hom} = \left[\frac{f_q}{\mu_q + b_0} + \frac{f_h}{\mu_h + b_0} + \frac{f_w}{b_0} \right]^{-1} - b_0 \quad (18)$$

where f is the volume fraction of a phase; the index q, h and w stand for quartz, gas hydrate and water, respectively; the bulk and shear moduli of the phases are given in Table 1. The volume fractions of the phases are related to the porosity and the hydrate saturation by:

$$f_q = 1 - \phi; f_h = \frac{S_h}{100}\phi; f_w = 1 - f_q - f_h \tag{19}$$

where ϕ is the initial porosity (porosity at zero hydrate saturation) and S_h (%) is the hydrate saturation.

Table 1 *: Elastic properties and densities of the phases of GHBS*

Phases	ρ (g/cm^3)	k (GPa)	μ (GPa)	Reference
Methal hydrate	0.9	7.9	3.3	Helgerud et al. (1999)
Quartz	2.65	37.8	44.3	Mavko et al. (2009)
Water	1.0	2.3	0.	Mavko et al. (2009)

In a common homogenization technique, a fixed homogenization scheme is usually chosen for a composite with a large range of microstructure change. However, it is well-known that each homogenization scheme can be used for just a certain small range of microstructure change. For example, the dilute and Mori-Tanaka schemes can be used for small to average amount of inclusions embedding in a matrix, the self-consistent scheme is appropriate for a randomly disordered mixture, *etc*. Here we propose to consider an adaptive homogenization scheme that allows a transition from one homogenization scheme to another. As previously discussed, the homogenization schemes are differed from each other by the parameters a_0 and b_0 of the reference matrix. Therefore we propose to adapt these parameters with the microstructure change; Nguyen et al. (2016) used this method for the effective transport properties of heterogeneous materials.

4.2. Calibration

Let consider the gas hydrate-bearing sand sample measured by Priest et al. (2005) of which the hydrate saturation, the volume fraction of water and both compression and shear sonic velocities were measured. For field application purpose, we consider the sample in water-saturated state, *i.e.* pore volume is filled by gas hydrate and water. Knowing the volume fraction of each phase, we compute the bulk density ρ by the following formula:

$$\rho = f_q\rho_q + f_h\rho_h + f_w\rho_w \tag{20}$$

Then the sonic velocities V_s and V_p is computed using the homogeneous bulk and shear moduli as:

$$V_s = \sqrt{\frac{\mu_{hom}}{\rho}};\ V_p = \sqrt{\frac{k_{hom} + \frac{4}{3}\mu_{hom}}{\rho}} \tag{21}$$

For this calibration step, we calibrate the parameters $\boldsymbol{a_0}$ and $\boldsymbol{b_0}$ to fit the data provided by Priest et al. (2005). Results are given in Table 2. It is of interest to note that these data have been obtained by converting measured data on unsaturated samples to equivalent saturated samples through the Gassmann's equation. As previously mentioned, the proposed model is calibrated for saturated samples due to field application purpose. However, the direct application of the model on unsaturated sample is mentioned later in section 4.4.

The following relation between the parameter b_0 and hydrate saturation S_h (%) is considered to fit the shear velocity (*Figure 3*):

$$b_0 = c_0\, \mathbf{log}_{10}\, S_h\,, \text{for } 1\% < S_h < 40\% \tag{22}$$

where $c_0 = 2.32$ for this case of gas hydrate sand formed by excess gas method (*Figure 3*). It is of interest to remark that for hydrate-free section ($S_h \leq 1\%$), rock is uncemented and unconsolidated then the Reuss approximation $b_0 = a_0 = 0$ (that corresponds to $S_h = 1\%$) is appropriate (Nur et al., 1991).

Then, to fit the compressional velocity (*Figure 4*), we consider a very simple relation:

$$a_0 = \frac{b_0}{2} \tag{23}$$

To summarize, for each sediment and at a given stress state, the model can predict the effect of the hydrate saturation on the sonic velocities by using only one fitting parameter c_0. The parameters a_0 and b_0 can be then determined by using the equations (22) and (23).

Table 2*: Sonic velocities of GHBS at different phases' volume fractions: a comparison between modeled and measured data.*

	Volume fractions				Modeled			Measured	
S_h (%)	f_w (V/V)	f_h (V/V)	f_s (V/V)	ρ (g/cm^3)	b_0 (GPa)	V_p (km/s)	V_s (km/s)	V_p (km/s)	V_s (km/s)
0.00	0.463	0.000	0.537	1.886	0.20	1.676	0.351	1.639	0.345
0.00	0.413	0.000	0.587	1.969	0.20	1.734	0.380	1.654	0.383
1.07	0.397	0.004	0.599	1.987	0.29	1.808	0.468	1.703	0.470
2.15	0.412	0.009	0.579	1.954	0.61	1.949	0.656	1.802	0.656
3.00	0.409	0.013	0.578	1.953	1.50	2.312	1.006	2.029	1.005
2.70	0.431	0.012	0.557	1.918	1.62	2.303	1.007	1.985	1.012
3.75	0.407	0.016	0.577	1.951	1.03	2.142	0.848	1.955	0.852
3.82	0.429	0.017	0.554	1.912	1.75	2.348	1.045	2.055	1.046

4.91	0.400	0.021	0.579	1.954	1.18	2.215	0.913	2.040	0.913
4.90	0.424	0.022	0.554	1.912	1.63	2.320	1.019	2.028	1.021
9.59	0.392	0.042	0.566	1.930	2.17	2.555	1.209	2.189	1.210
17.95	0.353	0.077	0.570	1.932	2.95	2.845	1.437	2.547	1.435
35.27	0.279	0.152	0.569	1.924	3.50	3.138	1.656	2.833	1.661

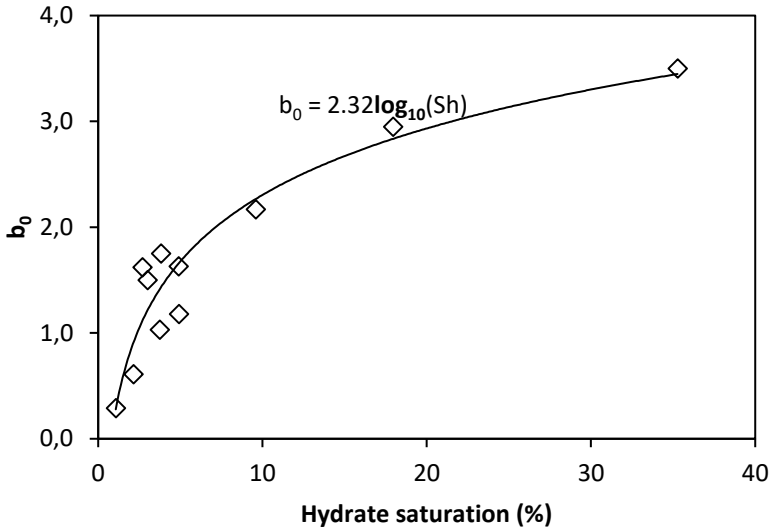

Figure 3: Dependence of the reference matrix on the microstructure: parameter b_0 versus hydrate saturation S_h.

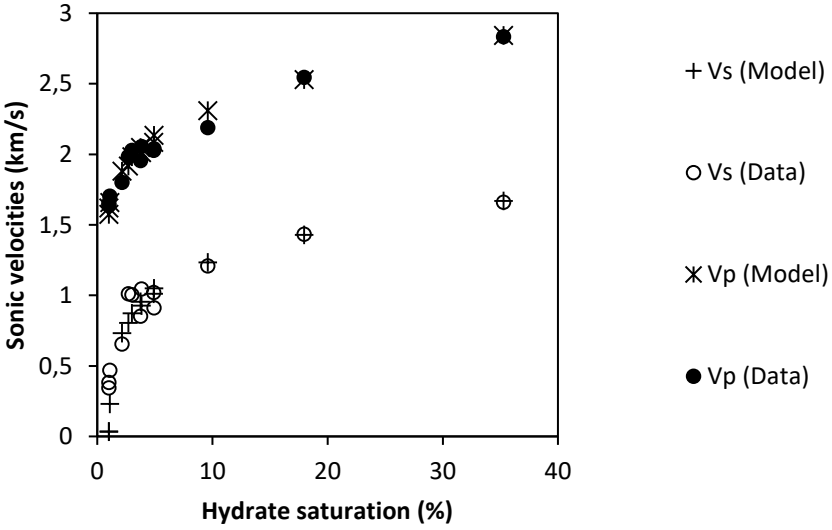

Figure 4: Sonic velocity of gas hydrate-bearing sand prepared in laboratory by the excess gas method : Experimental data (Priest et al. 2005) versus prediction by the present model. *Parameter:* $c_0 = 2.32$.

Figure 5 shows that a parameter $c_0 = 0.1$ allows a very good fit between the proposed method and data of gas hydrate-bearing sand formed by excess water method for a range of hydrate saturation below 40% (Priest et al., 2009). The parameter c_0 obtained for this case is very small comparing to the previous case of GHBS formed by excess gas method. So the parameter c_0 can be considered as a good indicator of GHBS formation and morphology.

On this figure, the results given by the existent model, that is a combination of the self-consistent (SC) and differential effective medium (DEM) schemes (Jakobsen et al., 2000; Hornby et al., 1994) (see also Appendix), are also ploted (called by SC-DEM model) for comparison. The model presented herein is obviously superior to the existent model. The existent SC-DEM model (Jakobsen et al., 2000) strongly over-estimates both compressional and shear velocities because it consider the self-consisent scheme for the mixture of quartz and water (at the first procedure before replacing little by little water by hydrate). Such technique can be used for a highly compacted sandstone but it is not appropriate for the samples measured by Priest et al. (2009).

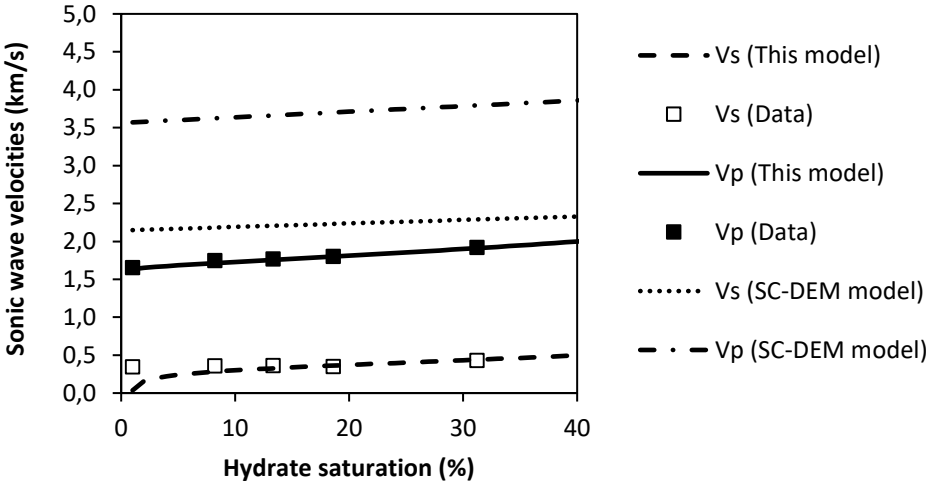

Figure 5: Validation of the model with experimental data of methane hydrate-bearing sand formed by the excess water method (Priest et al., 2009). Parameter: $c_0 = 0.1$.

The calibration of the relation (**22)** on the data of Priest et al. (2005) is limited to hydrate saturation lower than 40%. An additional calibration on data of Hu et al. (2012) shows that the relation between b_0 and S_h follows very well the trend defined by equation (**22)** for a hydrate saturation $S_h < 40\%$ but b_0 decreases linearly when S_h increases above 40% (*Figure 6*). Therefore, the following relation can be considered to predict b_0 for high degree of hydrate saturation:

$$b_0 = b_{40} - d_0(S_h - 40), \text{for } S_h > 40\% \quad (24)$$

where b_{40} is the value of b_0 at $S_h = 40\%$ that is computed by equation (**22)** and d_0 a constant. It is shown on (*Figure 7*) that the sonic wave velocities computed using equations (**17)** to (**24)**, with a calibrated parameter $c_0 = 0.95$ for $S_h < 40\%$ and a parameter $d_0 = 0.016$ for $S_h > 40\%$, fit very well the experimental data.

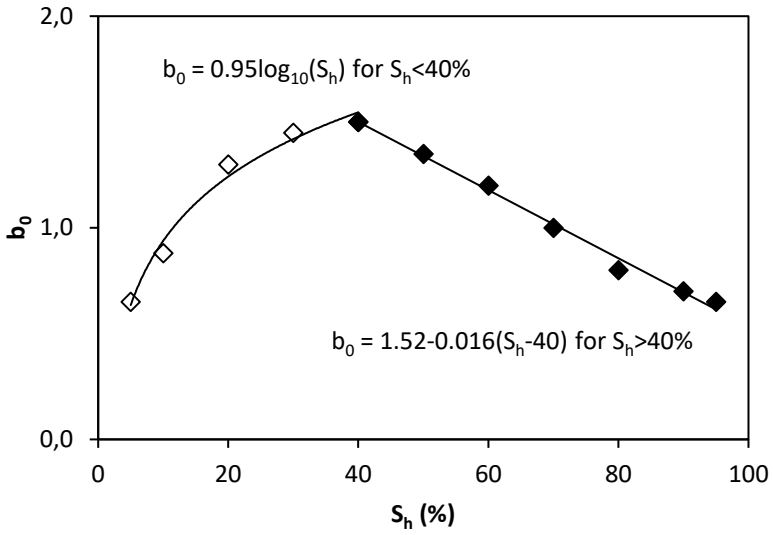

Figure 6: Parameter b_0 versus hydrate saturation S_h: calibration using data measured by the test "run 18" of Hu et al. (2012).

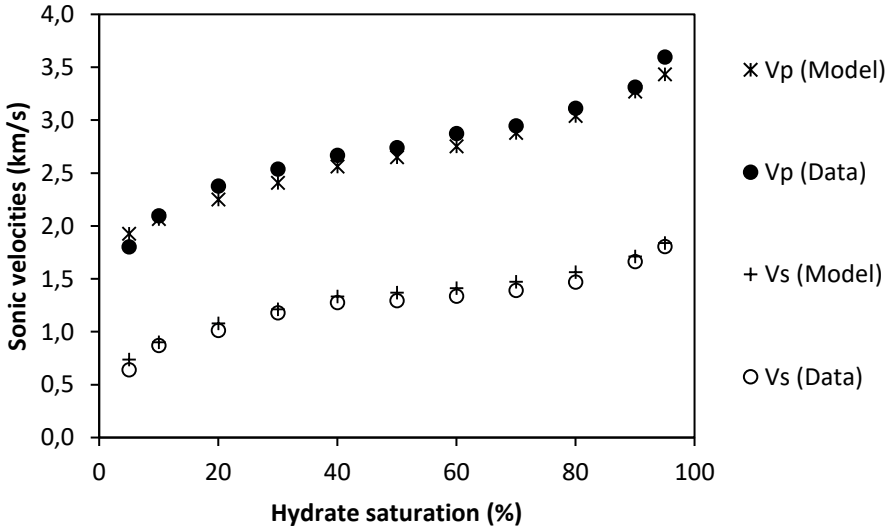

Figure 7 : A comparison between the proposed model and data measured by the test "run 18" of Hu et al. (2012). Parameters: $c_0 = 0.95$ and $d_0 = 0.016$.

4.3. Applications for natural GHBS

Konno et al. (2015) measured the compressional wave velocity of sediment samples containing methane hydrate cored under pressure from Japan offshore at about 300 ± 25 meters below sea-bed. Measurement were performed in side a aluminium pressure housing (Suzuki et al. 2015). To apply the proposed model to these natural samples containing other minerals beside quartz contents, additional terms are added to the formulas (**17)** and (**18)** as follows

$$k_{hom} = \left[\frac{f_q}{k_q + a_0} + \frac{f_{other}}{k_{other} + a_0} + \frac{f_h}{k_h + a_0} + \frac{f_w}{k_w + a_0}\right]^{-1} - a_0 \qquad (25)$$

and

$$\mu_{hom} = \left[\frac{f_q}{\mu_q + b_0} + \frac{f_{other}}{\mu_{other} + b_0} + \frac{f_h}{\mu_h + b_0} + \frac{f_w}{b_0}\right]^{-1} - b_0 \qquad (26)$$

where the parameters $k_{other} = 21$ (GPa) and $\mu_{other} = 7$ (GPa) given by Konno et al. (2015) are considered. The weight fraction of quartz in the mineral phases as well as the densities of quartz and other mineral given by Konno et al. (2015) are used to compute the volume fraction of quartz f_q and other mineral f_{other}. *Figure 8* shows the prediction values versus experimental data of Konno et al. (2015). Note that the porosities of the measured samples range from 32 % to 47 %. Therefore each modeled point on *Figure 8* corresponds to one sample. The parameters $c_0 = 0.1$ and $d_0 = 0$ are used for the simulation to fit all the data. We compare also the present model with the existent SC-DEM model (Jakobsen et al., 2000; Hornby et al., 1994). One more time we observe that the existent SC-DEM model over-estimates the compressional sonic wave velocity of hydrate bearing sediment while the model presented herein fits very well with experimental data.

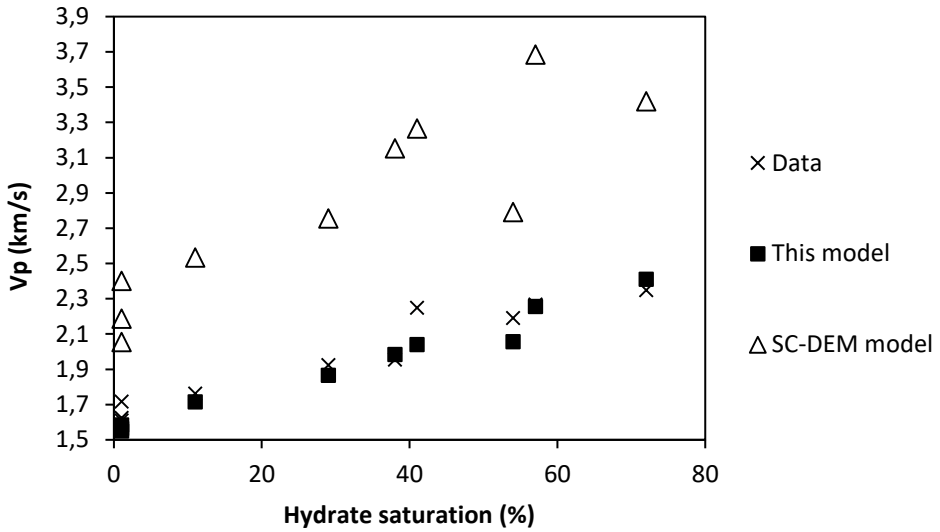

331

332 *Figure 8: Validation of the model with experimental data measured on natural methane*
333 *hydrate-bearing shaly sand (Konno et al., 2015). Parameter:* $c_0 = 0.1$ *and* $d_0 = 0$.

334

335 *Figure 9* shows the validation of the proposed model on log data given by Chand et al. (2004)
336 (where hydrate saturation was determined from electrical resistivity data and Archie's law). It
337 can be observed that the present model can predict correctly the magnitude and the high-
338 frequency variations of both V_p and V_s logs.

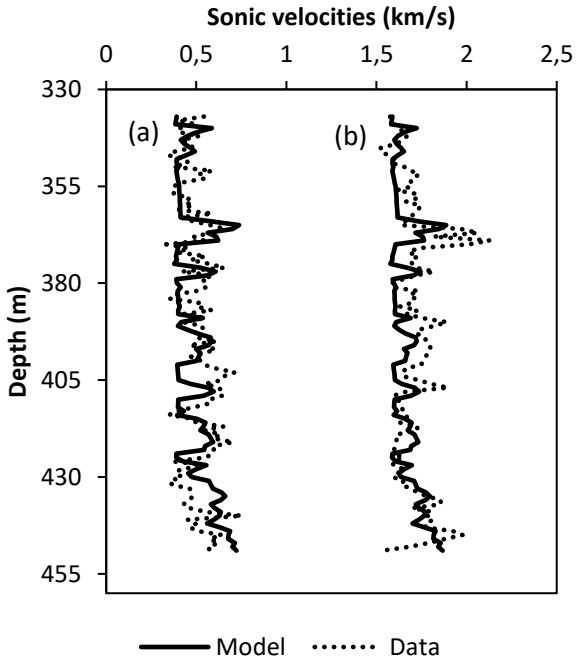

339

340 *Figure 9 : Validation of the model with log data of ODP Site 997, Blake Ridge, Leg 164 (see*
341 *Chand et al., 2004, figure 12): (a)* V_p *and (b)* V_s *versus depth. Parameter* $c_0 = 0.7$*, the*

parameter d_0 is not needed because the hydrate saturation is lower than 40%. The points with S_h close to 1 (%), leading to a negative or diverse value of b_0 (computed using equation (**22**)*), are not considered in the simulation.*

Wang et al. (2014) used multi-channel seismic reflection data, well logs, and recovered sediments cores to characterize the geologic control on the occurrence of gas hydrate in the Shenhu area of the South China Sea. Date available from Wang et al. (2014) at one site (SH2) are used to predict the compressional velocity log in the present work. *Figure 10* presents the results obtained by the prediction (with c_0 = 0.2; S_h < 40% in this work) and those measured from the field. It can be seen that the prediction is in good agreement with the measured values.

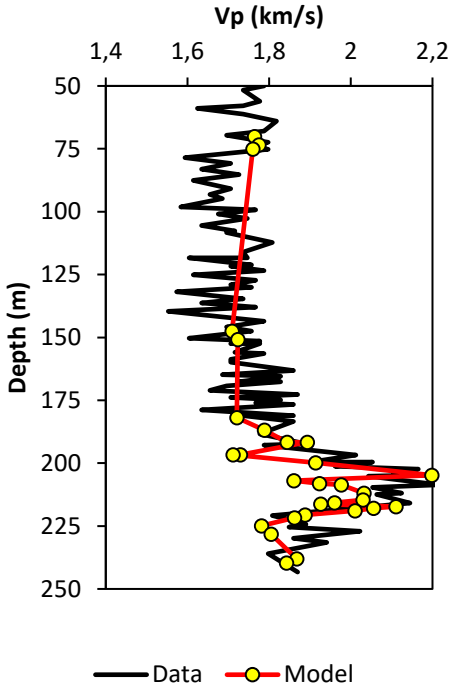

Figure 10 : Validation of the model with log data in the South China Sea (Wang et al., 2014, Well SH2). Parameter $c_0 = 0.2$.

Figure 11 shows a comparison between the proposed model and several existent key models given in litterature: Wood's equation (Wood, 1941); time-average equation (Wyllie et al., 1958) as well as the model proposed by Lee et al. (1996). We observe that these existent models can be fitted by the present method just by changing the parameter c_0. Consider for example a rock-bearing sandstone with an initial porosity of 57.5%, the Wood's method can be fitted by the proposed method herein by considering a parameter $c_0 = 0.05$ and $d_0 = 0.0004$.

Similarly, the time-average method can be fitted with $c_0 = 2.0$ and $d_0 = 0.002$. The results of Lee et al. (1996) with an exponent coefficient $n = 1$ can be fitted by using a parameter $c_0 = 0.8$ and a negative parameter $d_0 = -0.02$ (i.e. b_0 increases when S_h increases above 40%). It is also verified that the results obtained by Lee et al. (1996) with a parameter $n > 1$ can be fitted with a parameter c_0 between 0.8 and 2.0. It is of interest to remark that these existent models do not provide shear velocity while the present model provides both compressional and shear sonic velocities (*Figure 12*) with two calibration parameters c_0 and d_0.

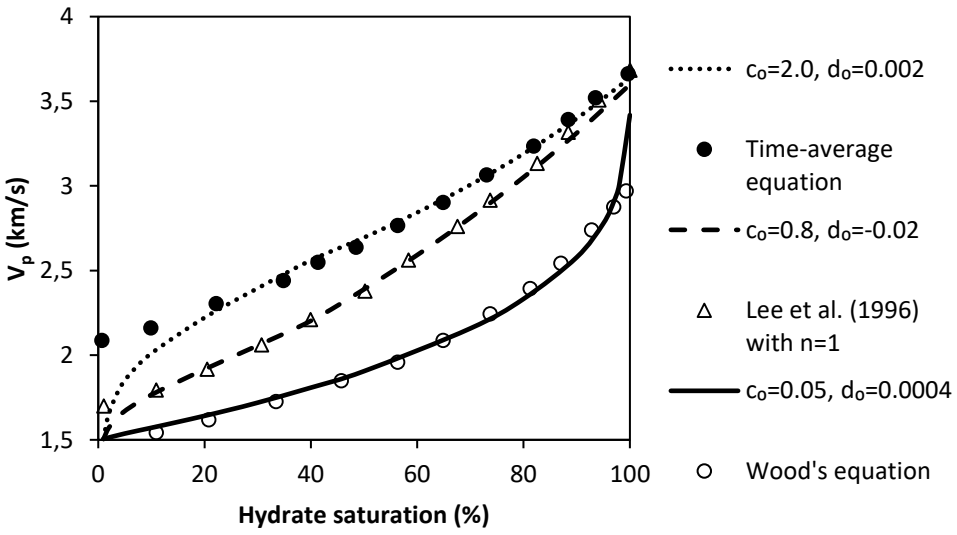

Figure 11 : Compression sonic velocity of GHBS versus its hydrate saturation with an initial porosity of 57.5%: a comparison between the proposed model and some existent models.

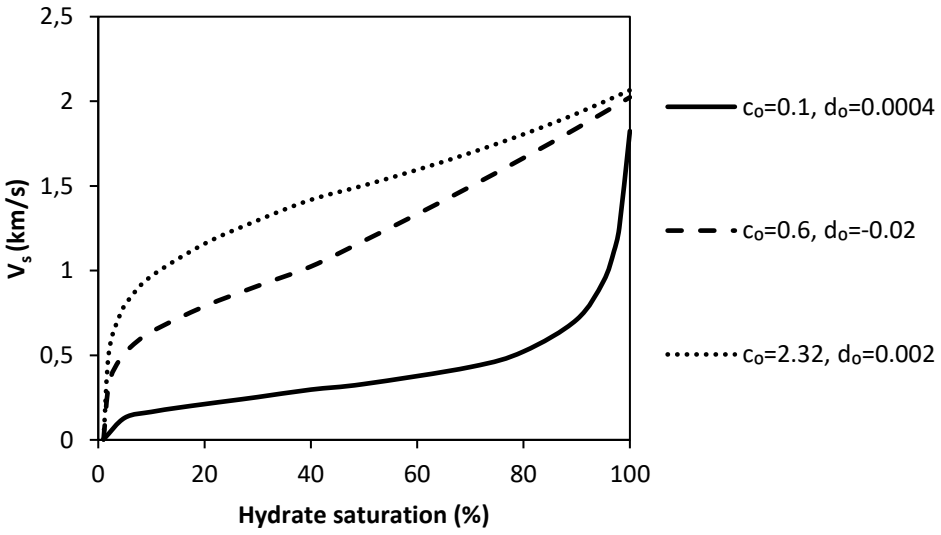

Figure 12 : Shear sonic velocity of GHBS versus its hydrate saturation with an initial porosity of 57.5%.

4.4.Unsaturated GHBS

Similar to the classical definitions of saturated or unsaturated rocks, here we employ the terms "partially saturated" or "unsaturated" for GHBS of which the pore space is not totally filled by water and hydrate but it is partially occupied by gas or air. Therefore the term "saturated" is used for GHBS with pore space totally filled by water and hydrate.

In section 4, we calibrate and validate a homogenization scheme that adapt with the microstructural change of saturated GHBS. With the case of unsaturated GHBS, it is necessary to add an additional terms related to air/gas phase in pore space to the formulas (**17)** and (**18)** as

$$k_{hom} = \left[\frac{f_q}{k_q + a_0} + \frac{f_{gas}}{a_0} + \frac{f_h}{k_h + a_0} + \frac{f_w}{k_w + a_0}\right]^{-1} - a_0 \tag{27}$$

$$\mu_{hom} = \left[\frac{f_q}{\mu_q + b_0} + \frac{f_{gas}}{b_0} + \frac{f_h}{\mu_h + b_0} + \frac{f_w}{b_0}\right]^{-1} - b_0 \tag{28}$$

The volume fraction of the phases are calculated by

$$f_q = 1 - \phi; f_{gas} = \frac{S_{gas}}{100}\phi; f_h = \frac{S_h}{100}\phi; f_w = 1 - f_q - f_h - f_{gas} \tag{29}$$

Note that equation (**20)** for the calculation of the bulk density remains valid due to almost zero density of air/gas phase. *Figure 13* shows a good fit between the prediction and data of dry gas hydrate sand measured by Priest et al. (2005) (direct measured data on dry sample, i.e. before transforming thought Gassmann calculation).

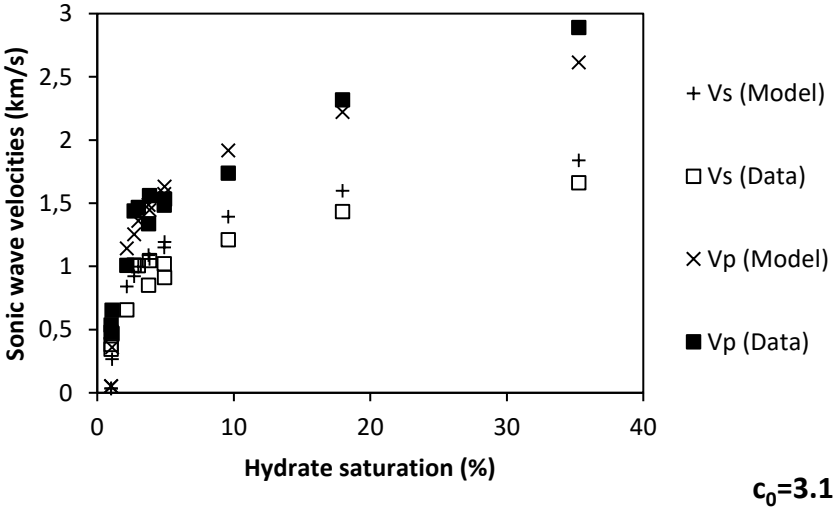

Figure 13: Sonic velocity of dry gas hydrate-bearing sand: Experimental data (Priest et al. 2005) versus prediction by the present model.

4.5. Sensitivity analysis

4.5.1. Influence of the initial porosity

Figure 14 shows the sensitivity of the initial porosity to the relationship between compression and shear sonic velocities versus hydrate saturation with fixed parameters $c_0 = 0.6$, $d_0 = 0$. For a porosity varies from 30% to 50% the compression sonic velocity decreases of about 10% to 15% and the shear velocity decreases of about 15% to 30% those are quite significant. However *Figure 14* shows that the sensitivity of the porosity to the relationship between the compression and the shear velocities are negligible, especially for a shear velocity higher that 1 (km/s) that corresponds to a hydrate saturation higher than 20%. The later explains a quite narrow trend of field data shown on *Figure 2* (filled circle points).

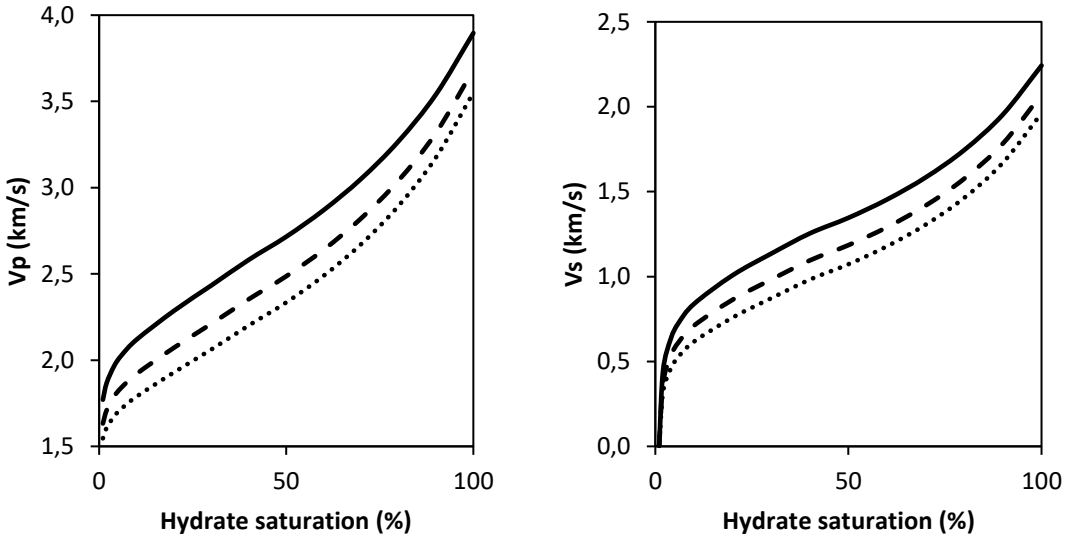

(a)

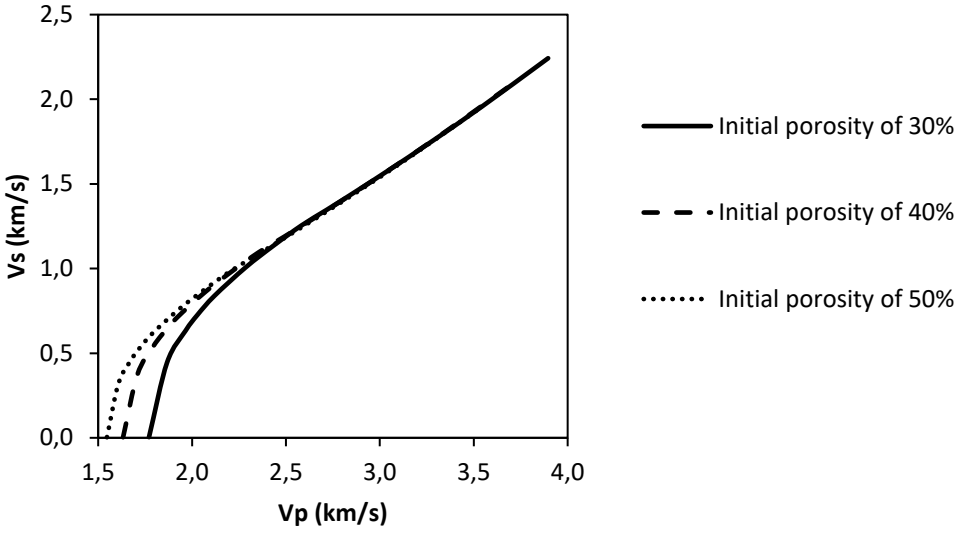

(b)

Figure 14 : Influence of the initial porosity on (a) Sonic velocities of GHBS versus its hydrate saturation; (b) Relationship between shear and compressional sonic velocities of GHBS.

4.5.2. Influence of the parameter c_0

Figure 15 shows a strong effect of the parameter c_0 on the relationships between the compressional and shear sonic velocities versus hydrate saturation with a porosity of $\phi = 0.4$ and a fixed parameter $d_0 = 0$. Therefore, to predict the hydrate saturation from sonic logs, it is important to correctly calibrate the parameter c_0. *Figure 16* shows that the relation V_p-V_s is also dependent on the parameter c_0.

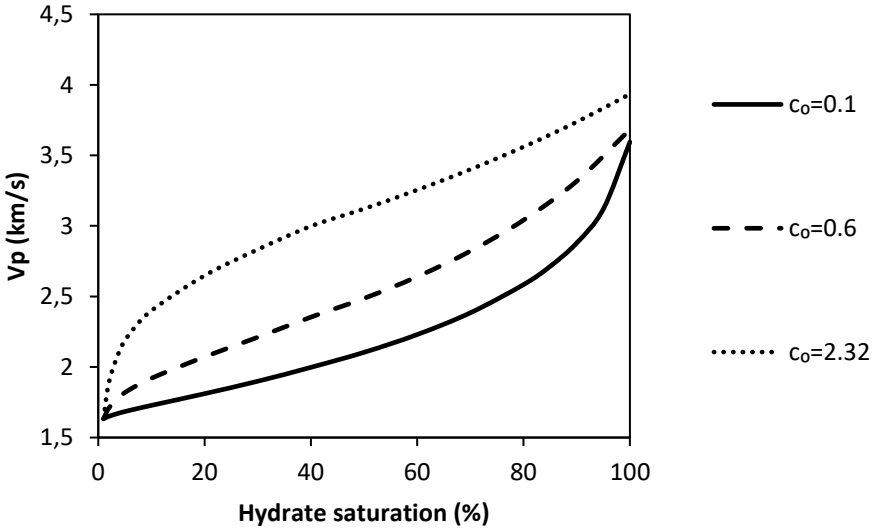

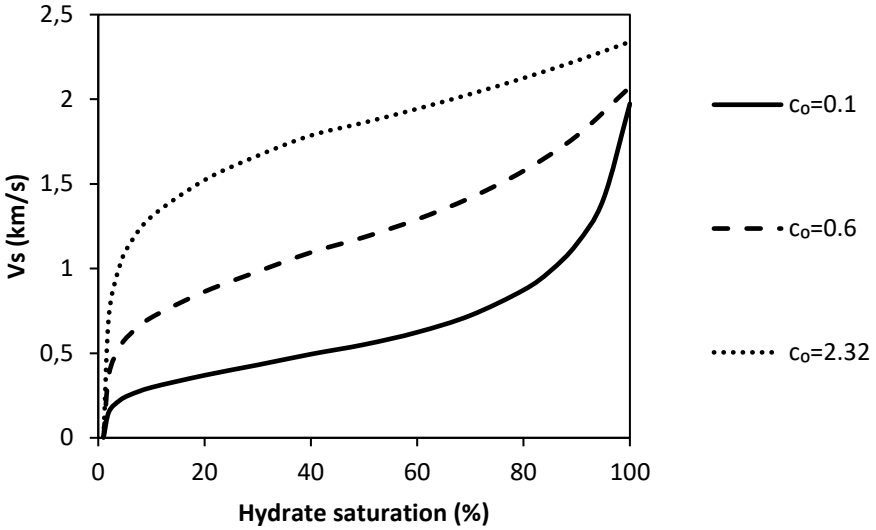

Figure 15 : Sonic velocities of GHBS versus its hydrate saturation for different values of c_0 in the range between 0.10 and 2.32 those are previously calibrated from laboratory data. Fixed parameters: $\phi = 0.4$ and $d_0 = 0$.

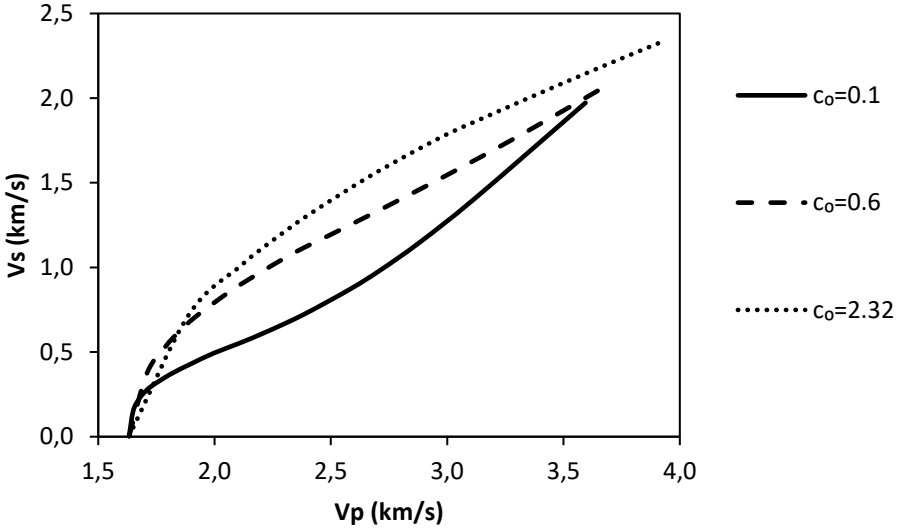

Figure 16 : Influence of the parameter c_0 on the relationship between shear and compressional sonic velocities of GHBS. Fixed parameters: $\phi = 0.4$ and $d_0 = 0$.

4.5.3. Influence of the parameter d_0

Figure 17 and *Figure 18* show a quite weak effect of the parameter d_0 on the relationships between the compressional and shear sonic velocities versus hydrate saturation with fixed parameters $\phi = 0.4$ and $c_0 = 1.0$. Besides, the in-situ hydrate saturation is usually

437 in the range below 40%. Therefore, the role of the parameter d_0 is less important than the
438 parameter c_0.

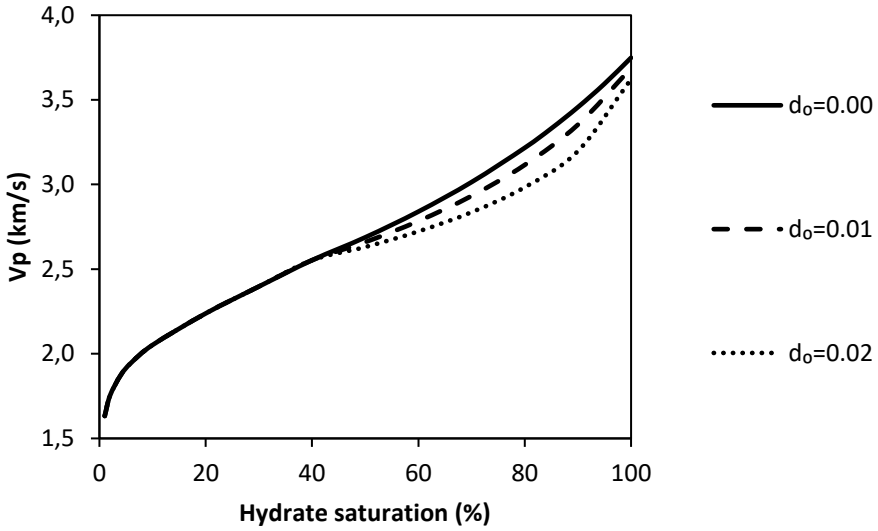

439

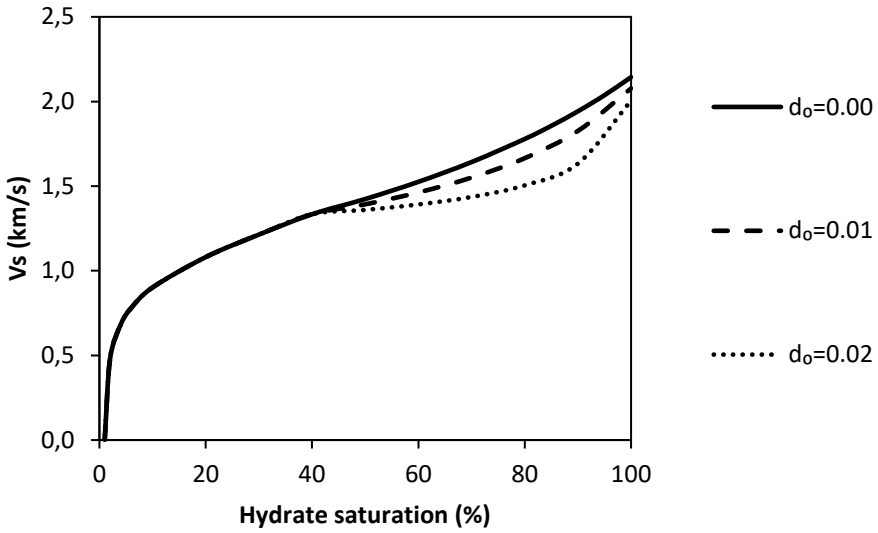

440

441 *Figure 17 : Sonic velocities of GHBS versus its hydrate saturation for different values of* d_0 *in*
442 *the range between 0 and 0.02 those are previously calibrated from data. Fixed parameters:*
443 $\phi = 0.4$ *and* $c_0 = 1.0$.

444

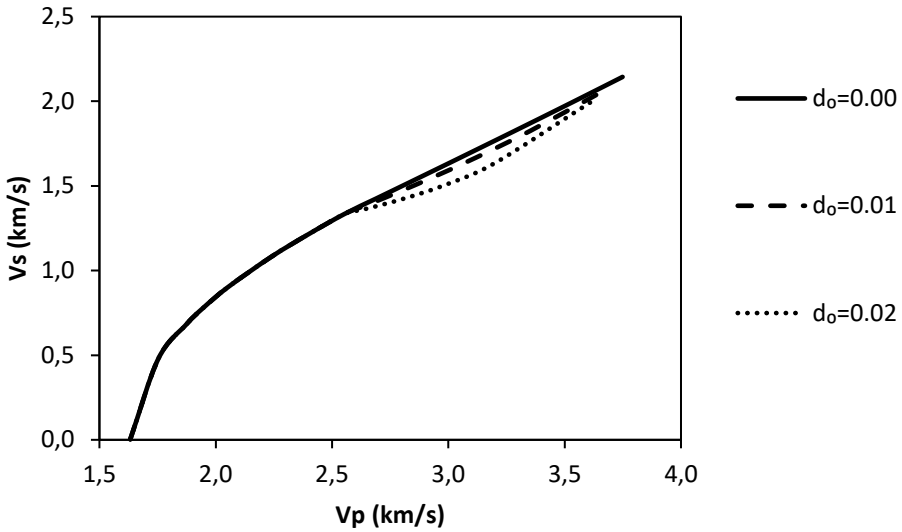

Figure 18 : Influence of the parameter d_0 on the relationship between shear and compressional sonic velocities of GHBS. Fixed parameters: $\phi = 0.4$ and $c_0 = 1.0$.

5. Concluding remarks

An adaptive homogenization scheme of which the elastic properties of the reference matrix are linearly related to the logarithm of hydrate saturation is proposed and calibrated for gas hydrate-bearing sand. The developed model can predict measured data just by changing two parameters c_0 and d_0. The parameter c_0 strongly depends on the morphology of the gas-hydrate phase. More precisely, c_0 is in a high range (about 2.0 to 3.0) if the gas-hydrate phase plays the role of the cement-phase that increases the stiffness of the rock frame. Inversely, for the case of weak GHBS, c_0 is in a low range (around 0.1) if the gas-hydrate phase plays the role of a pore-filling phase. Natural GHBS corresponds to a value in between these limits. Indeed, Nguyen et al. (2015) showed that an uncemented sand packing with a given porosity ϕ is as weak as a cemented one with a porosity of about 2ϕ.

The proposed model is validated with various experimental data obtained in laboratory including gas hydrate-bearing sands formed in laboratory, natural GHBS containing multi minerals. In addition, the prediction is also compared with the log data taken from various sites. All these validations evidence the robustness of the model.

When comparing the proposed model to the existing models, the proposed model is quite simple with two calibration parameters c_0 and d_0. In addition, it can predict both compression and shear sonic velocities within these parameters.

The results in the present work suggest that the calibration parameter c_0 would reflect the morphology of the GSBS. It is in a high range (around 2) if gas hydrates play the role of cement

phase while it is in a low range (around 0.1) if gas hydrates locate at the pore space between solid particles. The present model offers an easy and accurate technique to predict the hydrate saturation in GHBS using sonic logs and/or seismic acquisition.

Acknowledgements

The authors would like to express their great appreciation to the French National Research Agency for funding the present study, which is part of the project HYDRE "Mechanical behavior of gas-hydrate-bearing sediments" –ANR-15-CE06-0008. Related data of the paper are accessible by using the DOI: 10.6084/m9.figshare.6167717.

Appendix: the combined self-consistent and DEM method (Jakobsen et al., 2000; Hornby et al., 1994)

For low hydrate saturation, water is first mixed with the solid phase via the self-consistent scheme (see also Eqs. **(15)** to **(18)**)

$$k_{SC} = \left(\frac{\phi}{k_w + a_{SC}} + \frac{1-\phi}{k_q + a_{SC}} \right)^{-1} - a_{SC} \tag{30}$$

and

$$\mu_{SC} = \left(\frac{\phi}{\mu_w + b_{SC}} + \frac{1-\phi}{\mu_q + b_{SC}} \right)^{-1} - b_{SC} \tag{31}$$

with

$$a_{SC} = \frac{4}{3}\mu_{SC};\ b_{SC} = \frac{\mu_{SC}(9k_{SC} + 8\mu_{SC})}{6(k_{SC} + 2\mu_{SC})} \tag{32}$$

Once k_{SC} and μ_{SC} are determined, hydrate considered via a multi-step differential effective medium technique (DEM) that allows replacing little-by-little water in the pore space by hydrate. At a step i, the bulk and shear moduli can be computed by

$$k_{i+1} = \left[\frac{1}{k_i + a_i} + \frac{dv}{k_h + a_i} - \frac{dv}{k_w + a_i} \right]^{-1} - a_i \tag{33}$$

and

$$\mu_{i+1} = \left[\frac{1}{\mu_i + b_i} + \frac{dv}{\mu_h + b_i} - \frac{dv}{b_i} \right]^{-1} - b_i \tag{34}$$

where dv the increment of volume of water that is replaced by hydrate. The parameters a_i and b_i have a similar form of Eq. **(9)** as

$$a_i = \frac{4}{3}\mu_i;\ b_i = \frac{\mu_i(9k_i + 8\mu_i)}{6(k_i + 2\mu_i)} \tag{35}$$

At the first step, the effective bulk and shear moduli obtained by Eqs. **(30)** to **(32)** are used such as $k_0 = k_{SC}$ and $\mu_0 = \mu_{SC}$.

For high hydrate saturation (>50%), the effective bulk and shear moduli are calculated by a similar ways as the case of low hydrate saturation but the role of water and hydrate are interchanged. More precisely, the self-consistent procedure is first employed to mixe hydrate with the solid phase assuming 100% hydrate saturation. Then the DEM procedure is used to replacing litle by litle hydrate by water until reaching the desired hydrate saturation.

References

Carcione, J. M., & Tinivella, U. (2000). Bottom-simulating reflectors: Seismic velocities and AVO effects. Geophysics, 65(1), 54-67.

Chand, S., Minshull, T. A., Gei, D., & Carcione, J. M. (2004). Elastic velocity models for gas-hydrate-bearing sediments—A comparison. *Geophysical Journal International*, *159*(2), 573-590.

Chand, S., Minshull, T. A., Priest, J. A., Best, A. I., Clayton, C. R., & Waite, W. F. (2006). An effective medium inversion algorithm for gas hydrate quantification and its application to laboratory and borehole measurements of gas hydrate-bearing sediments. *Geophysical Journal International*, *166*(2), 543-552.

Choi, J. H., Dai, S., Cha, J. H., & Seol, Y. (2014). Laboratory formation of noncementing hydrates in sandy sediments. *Geochemistry, Geophysics, Geosystems*, *15*(4), 1648-1656.

Dormieux, L., Kondo, D., & Ulm, F. J. (2006). Microporomechanics. John Wiley & Sons, Chichester.

Dvorkin, J., & Nur, A. (1996). Elasticity of high-porosity sandstones: Theory for two North Sea data sets. *Geophysics*, *61*(5), 1363-1370.

Eshelby, J. D. (1957, August). The determination of the elastic field of an ellipsoidal inclusion, and related problems. In Proceedings of the Royal Society of London A: Mathematical, Physical and Engineering Sciences (Vol. 241, No. 1226, pp. 376-396). The Royal Society.

Freij-Ayoub, R., Tan, C., Clennell, B., Tohidi, B., & Yang, J. (2007). A wellbore stability model for hydrate bearing sediments. *Journal of Petroleum Science and Engineering*, *57*(1), 209-220.

Gassmann, F. (1951). Elastic waves through a packing of spheres. *Geophysics*, *16*(4), 673-685.

Guerin, G., Goldberg, D., & Meltser, A. (1999). Characterization of in situ elastic properties of gas hydrate-bearing sediments on the Blake Ridge. *Journal of Geophysical Research: Solid Earth*, *104*(B8), 17781-17795.

Han, D. H., Nur, A., & Morgan, D. (1986). Effects of porosity and clay content on wave velocities in sandstones. *Geophysics*, *51*(11), 2093-2107.

Hashin, Z., & Shtrikman, S. (1963). A variational approach to the theory of the elastic behaviour of multiphase materials. *Journal of the Mechanics and Physics of Solids*, *11*(2), 127-140.

Helgerud, M. B., Dvorkin, J., Nur, A., Sakai, A., & Collett, T. (1999). Elastic-wave velocity in marine sediments with gas hydrates: Effective medium modeling. *Geophysical Research Letters*, *26*(13), 2021-2024.

Hornby, B. E., Schwartz, L. M., & Hudson, J. A. (1994). Anisotropic effective-medium modeling of the elastic properties of shales. Geophysics, 59(10), 1570-1583.

Hu, G.W., Ye, Y.G., Zhang, J., Diao, S.B., & Liu, C.L. (2012). Acoustic properties of hydrate-bearing unconsolidated sediments measured by the bender element technique. *Chinese Journal of Geophysics*, 55(6), 635-647.

Jakobsen, M., Hudson, J. A., Minshull, T. A., & Singh, S. C. (2000). Elastic properties of hydrate-bearing sediments using effective medium theory. *Journal of Geophysical Research: Solid Earth*, *105*(B1), 561-577.

Johnson, A., Patil, S., & Dandekar, A. (2011). Experimental investigation of gas-water relative permeability for gas-hydrate-bearing sediments from the Mount Elbert Gas Hydrate Stratigraphic Test Well, Alaska North Slope. *Marine and petroleum geology*, *28*(2), 419-426.

King, M. S. (1984). The influence of clay-sized particles on seismic velocity for Canadian Arctic permafrost. Canadian Journal of Earth Sciences, 21(1), 19-24.

Konno, Y., Jin, Y., Yoneda, J., Kida, M., Egawa, K., Ito, T., ... & Nagao, J. (2015). Effect of methane hydrate morphology on compressional wave velocity of sandy sediments: Analysis of pressure cores obtained in the Eastern Nankai Trough. *Marine and Petroleum Geology*, *66*, 425-433.

Le, T. X., Rodts, S., Hautemayou, D., Aimedieu, P., Bornert, M., Chabot, B., & Tang, A. M. (2019). Kinetics of methane hydrate formation and dissociation in sand sediment. Geomechanics for Energy and the Environment. (doi: 10.1016/j.gete.2018.09.007)

Lee, M.W. (2008). Models for gas hydrate-bearing sediments inferred from hydraulic permeability and elastic velocities. *U.S. Geological Survey, Scientific Investigations Report*, 5219, 1-15.

Lee, M. W., Hutchinson, D. R., Collett, T. S., & Dillon, W. P. (1996). Seismic velocities for hydrate-bearing sediments using weighted equation. *Journal of Geophysical Research: Solid Earth*, *101*(B9), 20347-20358.

Lee, M. W., & Collett, T. S. (2001). Elastic properties of gas hydrate-bearing sediments. *Geophysics*, *66*(3), 763-771.

Lee, M. W. (2002). Biot–Gassmann theory for velocities of gas hydrate-bearing sediments. *Geophysics*, *67*(6), 1711-1719.

Li, Y. H., Song, Y. C., Yu, F., Liu, W. G., & Zhao, J. F. (2011). Experimental study on mechanical properties of gas hydrate-bearing sediments using kaolin clay. *China Ocean Engineering*, *25*(1), 113-122.

Mavko, G., Mukerji, T., & Dvorkin, J. (2009). The rock physics handbook: Tools for seismic analysis of porous media. Cambridge university press.

Milkov, A. V. (2004). Global estimates of hydrate-bound gas in marine sediments: how much is really out there?. *Earth-Science Reviews*, *66*(3), 183-197.

Mori, T., & Tanaka, K. (1973). Average stress in matrix and average elastic energy of materials with misfitting inclusions. Acta metallurgica, 21(5), 571-574.

Nguyen, S. T., Vu, M. H., & Vu, M. N. (2015). Equivalent porous medium for modeling of the elastic and the sonic properties of sandstones. Journal of Applied Geophysics, 120, 1-6.

Nguyen, S. T., Pham, D. C., Vu, M. N., & To, Q. D. (2016). On the effective transport properties of heterogeneous materials. International Journal of Engineering Science, 104, 75-86.

Nur, A., Marion, D., & Yin, H. (1991). Wave velocities in sediments. In *Shear waves in marine sediments* (pp. 131-140). Springer, Dordrecht.

Pham, D., Nguyen, Q., & Tran, A. (2017). Polarization approximations for elastic moduli of isotropic multicomponent materials. Journal of Mechanics of Materials and Structures, 12(4), 391-406.

Priest, J. A., Best, A. I., & Clayton, C. R. (2005). A laboratory investigation into the seismic velocities of methane gas hydrate-bearing sand. *Journal of Geophysical Research: Solid Earth*, *110*(B4) (doi:10.1029/2004JB003259).

Priest, J. A., Rees, E. V., & Clayton, C. R. (2009). Influence of gas hydrate morphology on the seismic velocities of sands. *Journal of Geophysical Research: Solid Earth*, *114*(B11) (doi:10.1029/2009JB006284).

Rees, E. V., Priest, J. A., & Clayton, C. R. (2011). The structure of methane gas hydrate bearing sediments from the Krishna–Godavari Basin as seen from Micro-CT scanning. *Marine and Petroleum Geology, 28*(7), 1283-1293.

Rutqvist, J., & Moridis, G. J. (2007, January). Numerical studies on the geomechanical stability of hydrate-bearing sediments. In *Offshore technology conference*. Offshore Technology Conference.

Rydzy, M. B. (2014). The effect of hydrate formation on the elastic properties of unconsolidated sediment (Doctoral dissertation, Colorado School of Mines. Arthur Lakes Library).

Shankar, U., & Riedel, M. (2014). Assessment of gas hydrate saturation in marine sediments from resistivity and compressional-wave velocity log measurements in the Mahanadi Basin, India. Marine and Petroleum Geology, 58, 265-277.

Sloan, E. D., & Koh, C. (2007). Clathrate hydrates of natural gases. CRC press.

Stern, L. A., Kirby, S. H., & Durham, W. B. (1996). Peculiarities of methane clathrate hydrate formation and solid-state deformation, including possible superheating of water ice. Science, 273(5283), 1843.

Sultaniya, A. K., Priest, J. A., & Clayton, C. R. I. (2015). Measurements of the changing wave velocities of sand during the formation and dissociation of disseminated methane hydrate. Journal of Geophysical Research: Solid Earth, 120(2), 778-789.

Suzuki, K., Schultheiss, P., Nakatsuka, Y., Ito, T., Egawa, K., Holland, M., & Yamamoto, K. (2015). Physical properties and sedimentological features of hydrate-bearing samples recovered from the first gas hydrate production test side on Daini-Atsumi Knoll around eastern Nankai Trough. *Marine and Petrolium Geology,* 66, 346 – 357.

Tan, C. P., Freij-Ayoub, R., Clennell, M. B., Tohidi, B., & Yang, J. (2005). Managing wellbore instability risk in gas hydrate-bearing sediments. In *SPE Asia Pacific Oil and Gas Conference and Exhibition*. Society of Petroleum Engineers.

Waite, W. F., Winters, W. J., & Mason, D. H. (2004). Methane hydrate formation in partially water-saturated Ottawa sand. American Mineralogist, 89(8-9), 1202-1207.

Waite, W. F., Santamarina, J. C., Cortes, D. D., Dugan, B., Espinoza, D. N., Germaine, J., ... & Soga, K. (2009). Physical properties of hydrate-bearing sediments. *Reviews of geophysics*, *47*(4).

Wang, X., Collett, T. S., Lee, M. W., Yang, S., Guo, Y., & Wu, S. (2014). Geological controls on the occurrence of gas hydrate from core, downhole log, and seismic data in the Shenhu area, South China Sea. Marine Geology, 357, 272-292.

Wood, A. B. (1941). A text book of sound. G. Bell and Sons, London.

Wyllie, M. R. J., Gregory, A. R., & Gardner, G. H. F. (1958). An experimental investigation of factors affecting elastic wave velocities in porous media. Geophysics, 23(3), 459-493.

Yun, T. S., Francisca, F. M., Santamarina, J. C., & Ruppel, C. (2005). Compressional and shear wave velocities in uncemented sediment containing gas hydrate. *Geophysical Research Letters*, *32*(10) (doi:10.1029/2005GL022607).

Zhang, Q., Li, F. G., Sun, C. Y., Li, Q. P., Wu, X. Y., Liu, B., & Chen, G. J. (2011). Compressional wave velocity measurements through sandy sediments containing methane hydrate. American Mineralogist, 96(10), 1425-1432.